INTERFEROMETERS

Interferometers are instruments that measure the phase difference of waves. They allow waves to propagate and interfere inside them and yield interference fringe patterns. From the fringe patterns that the interferometer gives one can determine the phase difference of waves and perhaps other parameters such as length, thickness, displacement, angular velocity, pressure, sound, temperature, magnetic field, and so on. This article concerns only optical interferometers. They are operated over the light (ultraviolet, visible, and infrared) wavelength range from several hundred nanometers to ten micrometers. Other interferometers such as microwave interferometers, radio interferometers, and x-ray interferometers also use electromagnetic waves. Their principles are similar to those of optical interferometers.

There are many kinds of interferometers, such as the Michelson–Mach, Zehnder, Fabry–Perot, and Sagnac interferometers. The widely used Michelson interferometer has two separate optical paths, as shown in Fig. 1(a). The light beam

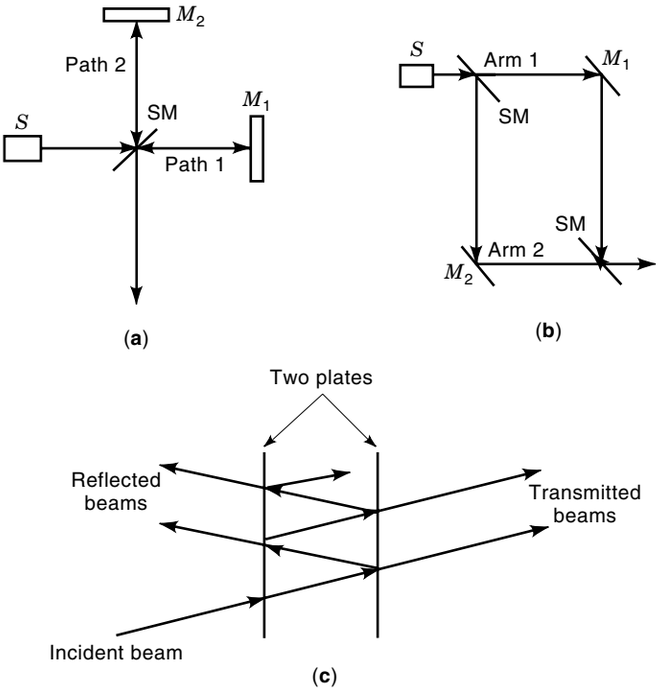

Figure 1. Three famous air-path interferometers. (a) The Michelson interferometer. (b) The Mach–Zehnder interferometer. (c) The Fabry–Perot interferometer. S, light source; SM, semireflecting, semitransmitting mirror; M_1, M_2, mirrors.

from the optical source S is split into two beams at the semireflecting semitransmitting mirror SM and propagate along paths 1 and 2, respectively. After being reflected by two mirrors M_1 and M_2, the two beams recombine at the semireflecting mirror SM to yield interference patterns. By moving the mirror in one path, one can change the phase difference of lightwaves in two paths and therefore find fringes shifting. The Michelson interferometer is often used to measure length, displacement, and many other parameters.

The Mach–Zehnder is another useful interferometer in numerous measurement fields. It can transmit more optical power emerging from the light source to the receiver than the Michelson interferometer. The Mach–Zehnder interferometer also has two separate light paths (more often called *arms*) as shown in Fig. 1(b). A light beam from the optical source S is split at the first semireflecting mirror into two beams. After propagating along the two arms, respectively, the two beams are recombined at the second semireflecting mirror to yield interference. The fringes will shift as the difference of the optical path lengths between arm 1 and arm 2 varies. Because the two arms are separate, various bulk modulators, e.g., electrooptic modulators, Bragg cells, and Faraday magnetooptic modulators, can be inserted in the optical paths. Modulators provide modulations in phase, frequency, and/or polarization states of light waves. They have played important roles in various detection systems.

The Fabry-Perot interferometer belongs to the multiple-beam category of interferometers and comprises two parallel partially transparent plates, as shown in Fig. 1(c). The light beam from the optical source passes through one plate at an angle and enters the cavity between the two plates. The beams are reflected between the two plates repeatedly, and when they emerge gradually from both sides of this cavity, called the Fabry–Perot cavity, they form, respectively, two types of multiple-beam interference fringe patterns. This kind of interferometer produces sharp fringes owing to the multiple reflection. The half-width of the bright fringe is related to the reflectivity of the inner surface of the plate. The higher the reflectivity, the narrower the half-width. The Fabry–Perot interferometer is useful for temperature measurement, optical filtering, and the study of the fine structure of spectrum lines.

Fiber-optic interferometers have formed a rather large and important category among the various interferometers. In fiber-optic interferometers, the lightwave propagates in the optical fiber rather than in the air. As the fiber is flexible, the direction of the light propagation can vary continuously, which is impossible for air-path interferometers. Environmental factors can influence the fiber by changing its dimensions and the refractive indices of its materials, and therefore result in the variations in the phase difference and the polarized state of lightwaves. These influences cause noises and errors in measurements, but on the other hand, they offer the fundamentals of various sensing schemes (1). The relation between the light phase shift and the external factor is quite complicated in practical situations. It depends on the nature of the measurand and the material and structure of the fiber used. The fiber-optic interferometer generally uses a single-mode optical fiber, permitting only one mode to propagate inside it. There is birefringence in the practical fiber that produces the two orthogonal polarization waves that propagate with different phase velocities. Perturbations couple the two polarization modes and thus give noise at the output. The use of the high-birefringence fiber can prevent coupling between the two modes.

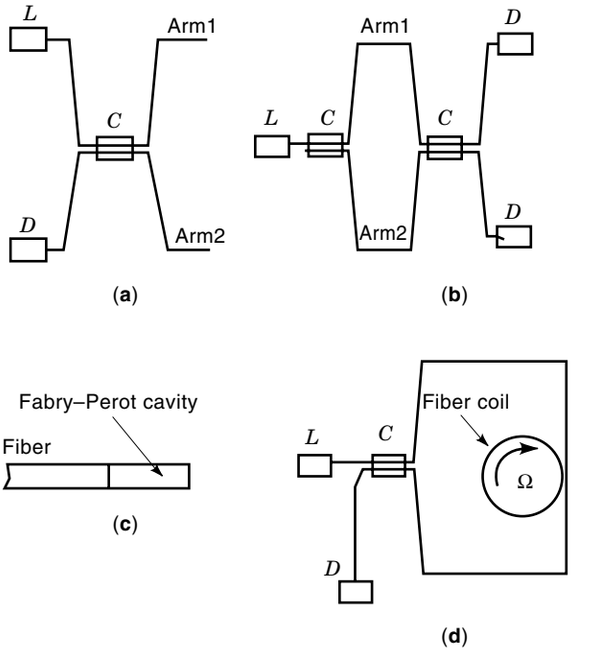

Figure 2. Four famous fiber-optic interferometers. (a) The fiber-optic Michelson interferometer. (b) The fiber-optic Mach–Zehnder interferometer. (c) The fiber-optic Fabry–Perot interferometer. (d) The fiber-optic Sagnac interferometer. L, laser; C, coupler; D, photodetector.

Much effort has been spent to apply fiber-optic interferometers to pressure, strain, temperature, acoustic wave, magnetic field, and rotation rate measurements (2). Figure 2 shows schematically several useful fiber-optic interferometers. In these arrangements, bulk devices such as semireflecting mirrors and modulators are replaced by their waveguide counterparts. The measurands induce the phase shift of the signal arm. Fiber-optic interferometers usually use the phase modulators to improve their performance. The phase modulator changes the optical path length of the reference arm and leads to the phase shift of the light wave. As the length of the fiber in the measurand field can be increased readily, the fiber-optic interferometer is apt to reach higher measurement sensitivity than the air path interferometer.

The principle of the fiber-optic interferometer is similar to that of its air path counterpart. Fig. 2(a) shows the fiber-optic Michelson interferometer. The optical beam from a laser launches to the coupler and divides into two beams there. After being modulated in each arm by measurand and modulator, respectively, the two beams recombine at the same coupler and give rise to interference. Compared with the fiber-optic Michelson interferometer, the fiber-optic Mach–Zehnder interferometer has two couplers, as shown in Fig. 2(b). The coupler at which the two light beams are recombined is different from the one at which the light beam is split. Obviously, as the phase difference varies, the output of the photodetector varies.

Figure 2(c) shows the basic configuration of the fiber-optic Fabry–Perot interferometer. There are two reflecting faces inside the optical fiber. In many cases, one reflecting face is just

the surface end of the fiber. The fiber portion between the two reflecting faces constitutes a Fabry–Perot cavity. When the measurand changes the optical path length of the cavity, the phase difference of light beams proceeding to the photodetector is changed.

The fiber-optic Sagnac interferometer has a common ring path for two optical beams propagating in opposite directions. Nonreciprocal factors such as rotation rate generate a nonzero phase difference between the two light waves. As shown in Fig. 2(d), light from the optical source is split at the coupler into two beams, which then counterpropagate in the fiber coil. When the fiber coil rotates clockwise about its axis, the clockwise light beam takes a longer time to travel between two fixed points in the fiber coil than the anticlockwise light beam. So there exists a nonzero phase difference between the two counterpropagating lightwaves. This interferometer can be used for inertial navigation as a gyroscope.

The properties of light sources and photodetectors play important roles to interferometer performances (1–3). In most cases, interferometers use lasers as their optical sources because the laser light has a good spatial coherence and a good temporal coherence. Both light sources and photodetectors can introduce noises. There are many noises in interferometers, such as shot noise, thermal noise, $1/f$ noise, mode-mode interfering noise, and so on, which produce errors in output. Perturbations due to the fluctuation in the optical source intensity and the variation in the polarized state of lightwaves also result in errors. A well-designed setup and an appropriate detection scheme can reduce the influences of noises. There are numerous detection schemes, and many of them suit more than one interferometer.

BASIC FORMULAE FOR INTERFERENCE

The interference of two light waves gives a superposed optical field as follows

$$\boldsymbol{E}(t) = \boldsymbol{E}_1(t) + \boldsymbol{E}_2(t)$$

where $\boldsymbol{E}_1(t)$ and $\boldsymbol{E}_2(t)$ represent the optical vectors of the two light waves to be superposed. The fringe intensity as well as the output of the photodetector depends on *the optical power* of the light wave rather than the instantaneous value of the amplitude of the light wave. Thus the fringe intensity can be written as (4)

$$I = I_0 + I_0 \mathscr{V} \cos\phi$$

Here ϕ denotes the phase difference of the two light waves, I_0 is a constant proportional to the light source intensity, and $\mathscr{V}$ gives the interference term that is related to the mixing efficiency. The fringe intensity depends on the phase difference ϕ. When $\phi = m\pi$, $|m| = 0, 1, 2, \ldots, I$ reaches its maximum I_a, and when $\phi = m\pi$, $|m| = \frac{1}{2}, \frac{3}{2}, \frac{5}{2}, \ldots, I$ equals minimum I_i. The distinctness of the fringe pattern can be specified by *the visibility of fringe* or *the fringe contrast* that is defined as $(I_a - I_i)/(I_a + I_i)$.

The visibility of fringe is related to the spatial coherence, the temporal coherence, and the polarized direction of the light waves used. *Spatial coherence* describes how close a practical light source approaches a point optical source. When a practical light source is an extended one, the different points in the source will produce different light waves with different phases at the observing point. Thus the interference effect due to one emitting point of the light source may be counteracted partially by another point of the light source, which results in the decrease of the visibility of fringe. On the other hand, when the light wave from the optical source is not a strictly monochromatic one, the visibility of fringe will decrease even if the light source is a point source in the case that the phase difference of light waves is large. *Temporal coherence* describes how near a practical light source approaches a monochromatic optical source. According to quantum mechanics, the light wave emerging from an atom is a wave train with a finite length in the time axis. This temporal finite length is called *coherence time.* The interference will occur when light wave trains are overlapped partially, that is, when the time difference of the light wave trains is less than the coherence time. There is a relation between the coherence time $\Delta\tau$ and the spectral width $\Delta\omega$ of the light which can be written as

$$\Delta\tau\Delta\omega \geq 1$$

which means that the wave train is not infinitely long unless the light is a strictly monochromatic one. Another important parameter specifying the temporal coherence is the *coherence length* l_c, which is defined as

$$I_c = c\Delta\tau$$

where c is the velocity of light. Generally speaking, the visibility of the fringe will be reduced as the difference between the optical paths increases, and will approach zero as such difference becomes much greater than the coherence length. However, practical experiments show that even if the path difference is several times longer than the coherence length, the interference effects can still be seen (2).

The polarized directions of the light waves can also affect the visibility. For the linearly polarized situation, when the polarized planes of the two superposed light waves are parallel, $\mathscr{V}$ has a maximum value; whereas when they are orthogonal, $\mathscr{V}$ becomes zero.

CONFIGURATIONS, PRINCIPLES, AND APPLICATIONS OF INTERFEROMETERS

Michelson Interferometer

The Michelson interferometer is shown schematically in Fig. 3. Light waves propagating along paths one and two are recombined at the semireflecting mirror or the coupler to give rise to interference fringe. Under illumination by an extended source, the interference produces fringes of equal inclination localized at infinity if the mirror M_2 and the image of the other mirror M_1 are parallel, and fringes of equal thickness localized near M_2 if they are mutually inclined at a small angle. When the interferometer is illuminated by a white-light source, one can see only zeroth-order fringe and some low-order fringes. High-order fringes are invisible because of the short coherence length of the white light. The fringe pattern can be converted into current or voltage by use of the photodetector. The output of the photodetector that responds to the optical intensity of the fringe will vary as the mirror moves. Obviously the output of the photodetector has a one-cycle variation as the mirror moves a distance equal to half

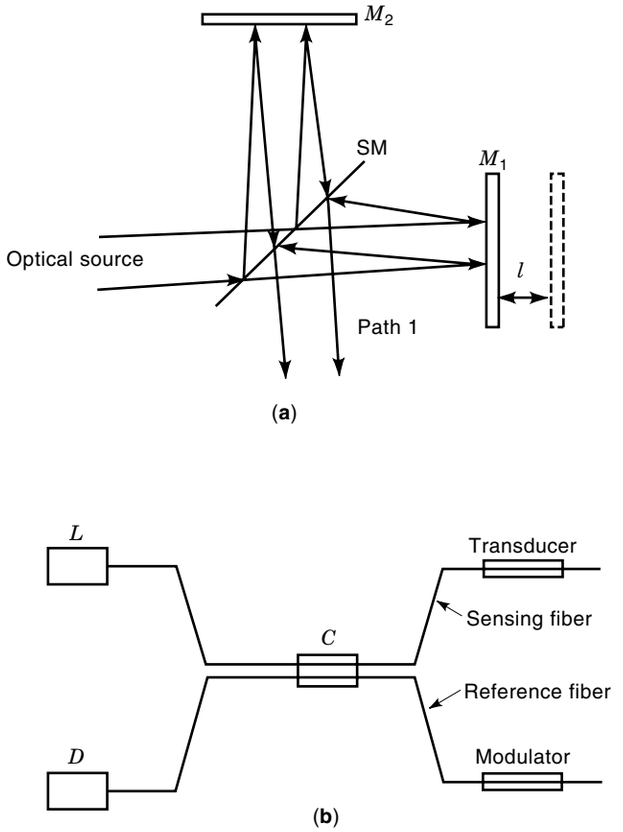

Figure 3. (a) The air-path Michelson interferometer that measures displacement of the plate M_1. (b) The fiber-optic Michelson interferometer that is used as the interferometric sensor. L, laser; SM, semireflecting, semitransmitting mirror; M_1, M_2, mirrors; C, coupler; D, photodetector.

an optical wavelength $\lambda/2$. When the difference of the optical path length between paths 1 and 2 equals $m\lambda$ where $|m| = 0$, 1, 2, . . ., the output of the photodetector reaches its maximum, and when such difference equals $m\lambda$ where $|m| = 1/2$, 3/2, . . ., the output of the photodetector reaches its minimum (4). Measuring these electric signals, one can obtain at least $\lambda/2$ or 300 nm of displacement resolution.

For the fiber-optic Michelson interferometric sensor, the variation measurand alters the length, diameter, and refractive index of the sensing fiber and thus results in the phase shift of the light wave. Take the temperature measurement as an example. In this case, the sensing fiber is attached to the thermal-sensitive material, whereas the reference fiber is attached to the thermal nonactive material. The variation in temperature makes the sensing material as well as the sensing fiber spread and contract so that the phase difference is changed. This kind of thermometer can attain a sensitivity of the order of 1×10^{-5} K (5).

The Michelson interferometer can be used to measure displacement, length, temperature, pressure, gas flow, spectrum distribution, and many other factors.

Mach–Zehnder Interferometer

Figure 4 shows the schematic of a typical Mach–Zehnder interferometer. The output of the photodetector reaches its maximum when the difference of the optical path lengths nl between two arms 1 and 2 satisfies

$$nl = m\lambda, |m| = 0, 1, 2, \ldots$$

and minimum when nl satisfies

$$nl = m\lambda, |m| = 1/2, 3/2, 5/2, \ldots$$

where n is the refractive index and l is the path difference of the two arms (1).

For the fiber-optic Mach–Zehnder or other type of interferometers, the detectable phase shift usually has to be as small as 10^{-6} rad or less. Thus the noises caused by lasers, photodetectors, and other components cannot be ignored (2,3). For a stable and reliable readout, an appropriate detection scheme is necessary.

The detection schemes can be classified as homodyne with phase tracking, homodyne without phase tracking, and heterodyne. The homodyne (3) detection system is illustrated in Fig. 5. The output voltages (or currents) of the photodetectors are of the form for this case

$$\begin{aligned} V_1 &= V_0[1 + \gamma \cos(\phi_s - \phi_r + \phi_n)] \\ V_2 &= V_0[1 - \gamma \cos(\phi_s - \phi_r + \phi_n)] \end{aligned} \tag{1}$$

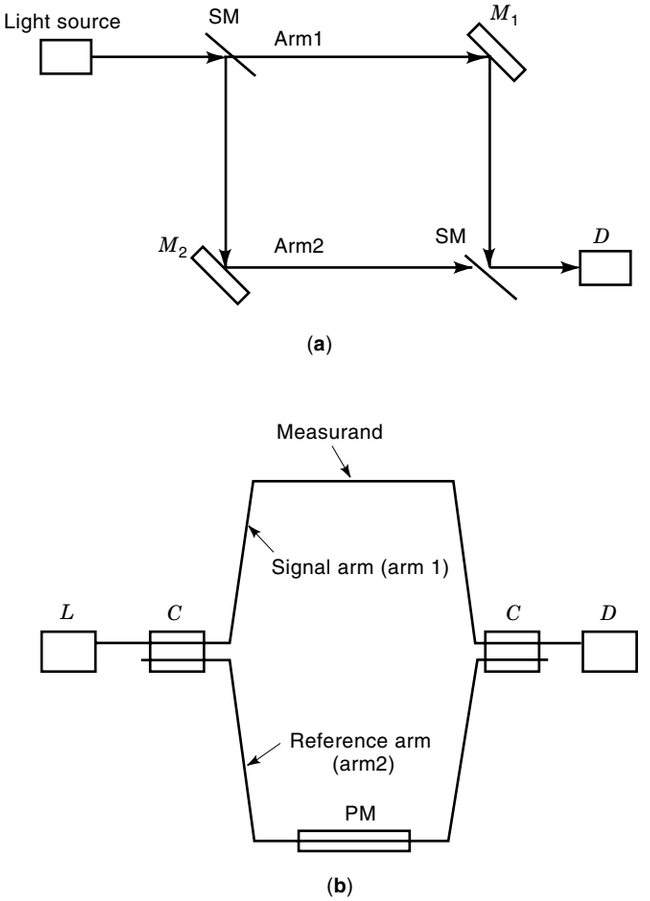

Figure 4. The Mach–Zehnder interferometer, which can transmit more optical power to the photodetector than the Michelson interferometer. (a) The air-path. (b) The fiber-optic. L, laser; SM, semireflecting, semitransmitting mirror; M_1, M_2, mirrors; C, coupler; D, photodetector; PM, phase modulator.

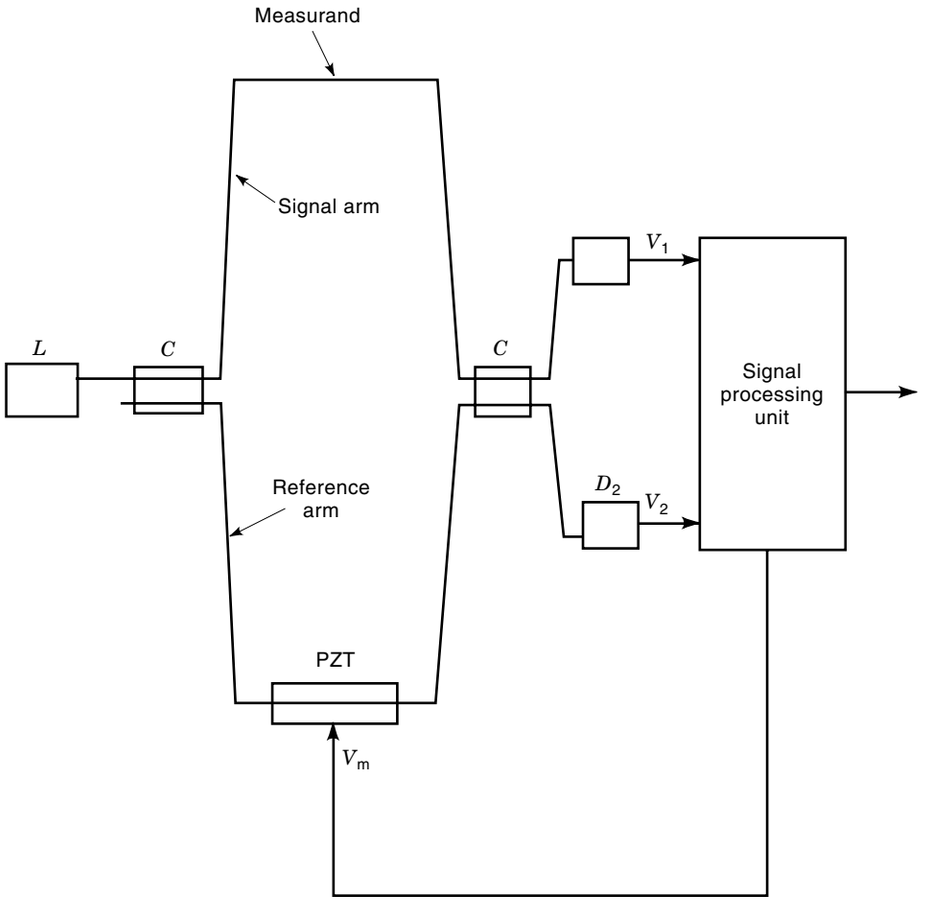

Figure 5. The basic form of the phase-tracking homodyne system. L, laser; C, couplers; D_1, D_2, photodetectors.

where ϕ_s is the phase shift in the signal arm induced by the measurand, ϕ_r is the phase shift in the reference arm produced by modulation, and ϕ_n is the phase difference between the two arms that is due to noise and other disturbance. In this case, V_0 is the constant proportional to the optical power of the laser. γ is the parameter related to fringe contrast. To obtain the maximum sensitivity, the system should satisfy the quadrature condition, that is, $\phi_s - \phi_r + \phi_n = 2m\pi \pm \pi/2$. The phase-tracking homodyne scheme uses the feedback control technique to maintain the quadrature condition. The electronic circuit transforms V_1 and V_2 into the feedback voltage V_m that applies to the piezoelectric transducer (PZT) device to stretch the reference arm to change ϕ_r. Under the quadrature condition, V_1 and V_2 are proportional to the phase shift induced by the measurand, approximately if this phase shift is small.

Besides the above dc modulation manner, the interferometer can be operated in the dc-ac hybrid modulation way. In this case, V_m is the sum of dc and ac voltages. The dc voltage produces a dc phase bias to maintain quadrature condition, and the ac voltage induces a phase variation with the modulation frequency to facilitate phase detection. The output V_1 can be achieved by J_1(max) method (6). One advantage of this ac modulation is the attainable high SNR because of the possible use of the lock-in amplifier in the system. Both the dc modulation scheme and the dc-ac hybrid scheme have drawbacks. They have resetting noise and are complicated in structure. However, in practice, the phase-tracking schemes can work quite well.

The no-phase-tracking homodyne system does not need feedback control. In contrast to the phase-tracking homodyne arrangement, the no-phase-tracking homodyne arrangement has a rather simple structure. It avoids the reset problem involved in the phase tracking operation. There are many no-phase-tracking homodyne schemes. Figure 6(a) shows schematically the system using a 3×3 coupler. The beams along the two arms recombine together at the 3×3 coupler instead of at a 2×2 coupler and give rise to outputs different from those given by Eq. (1). Through signal processing with appropriate electronic circuits, a result proportional to the phase difference is achieved. It has been reported that a minimum detectable phase shift of 3×10^{-6} rad at 1 kHz and a dynamic range of 10^7 were attainable for this detection scheme (7).

Figure 6(b) shows another no-phase-tracking homodyne scheme, called homodyne demodulation. The output of the photodetector V_1 in this case has the same form as that in Eq. (1). Because of the ac modulation, V_1 can be written as

$$V_1 = V_0 + V_0\gamma\{[J_0(M) - 2J_2(M)\cos 2\omega_m t + \cdots - \cdots]\cos(\phi_s + \phi_n) + [2J_1(M)\cos\omega_m t - \cdots + \cdots]\sin(\phi_s + \phi_n)\} \quad (2)$$

where J_i denotes the Bessel function of order i, and M is modulation depth. Multiplying the first harmonic (ω_m) by the derivative of the second harmonic ($2\omega_m$), then subtracting the product of the second harmonic and the derivative of the first harmonic, and finally integrating this difference, one can obtain a result varying directly with ($\phi_s + \phi_n$). As the signal ϕ_s and the noise ϕ_n are usually within different bands, it is not

difficult to remove ϕ_n by filtering. Dandridge et al. have shown that the detectable phase shift of 10^{-6} rad at 1 kHz was attainable with this scheme (8).

The $J_1 \ldots J_4$ method is also a useful no-phase-tracking homodyne scheme, as shown in Fig. 6(b). The ac phase modulation is not necessary here where the interferometer is used to measure dynamic phase changes. The output of the photodetector D has a form similar to that of Eq. (2). According to the recurrence relation of the Bessel functions, the following expression can be obtained

$$X^2 = 4i(i+1)V(i)V(i+1)/\{[V(i)+V(i+2)][V(i-1)+V(i+1)]\}$$

Here X is the modulation depth induced by the measurand and $V(i)$ is the voltage amplitude of the ith frequency component of the output voltage of the photodetector. This approach has removed the need of stabilizing the source intensity and polarization control, which is welcome in practical applications (9).

The heterodyne detection system uses frequency modulators to produce a frequency shift. The output of the photodetector is an FM signal in this case. It has the form of

$$V_o = 2V_0 \gamma \cos[(\omega_s - \omega_r)t + \phi_s(t) + \phi_n]$$

where ω_s and ω_r are two angular frequencies of light waves in the signal arm and the reference arm, respectively.

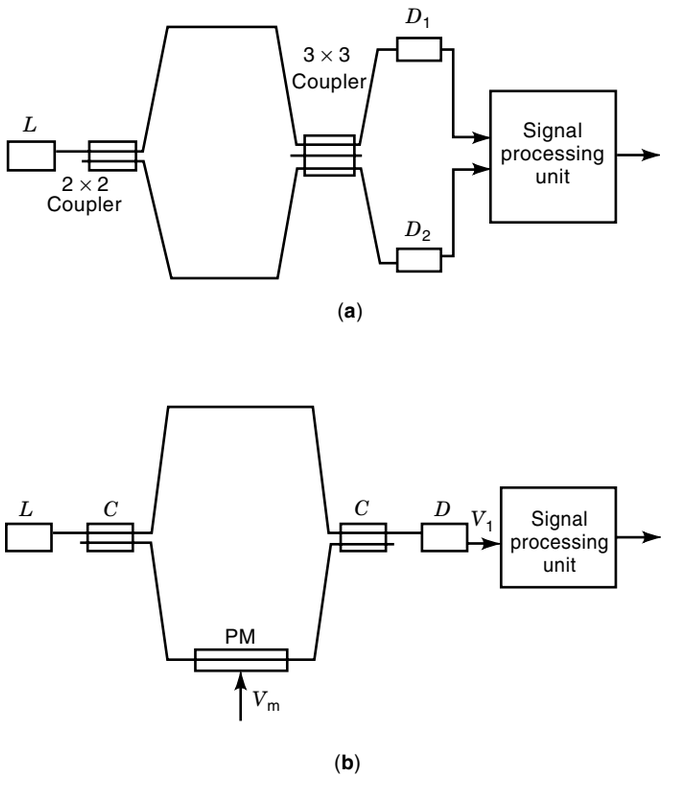

Figure 6. (a) The no-phase-tracking homodyne system using 3 × 3 coupler. (b) The passive homodyne system using demodulation or $J_1 \ldots J_4$ method. L, laser, C, 2 × 2 couplers; D, D_1, D_2, photodetectors; PM, phase modulator.

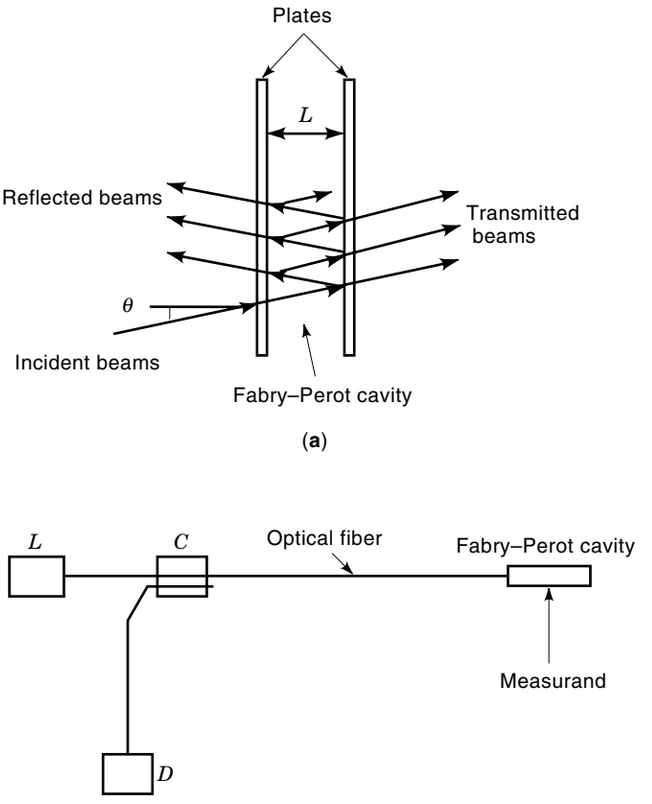

Figure 7. (a) The Fabry–Perot interferometer. (b) The basic configuration of fiber-optic Fabry–Perot interferometric sensor. L, laser; C, coupler; D, photodetector.

Another heterodyne system is called synthetic heterodyne system. This system uses the PZT element as the frequency modulator. The output signal of the interferometer is calculated or "synthesized" before entering the FM discriminator. The processed signal has the form of

$$V_s = 2V_0 \gamma J_1(M)\cos(3\omega_m t + \phi_s + \phi_n)$$

The advantage of the heterodyne scheme is that neither feedback circuit nor resetting arrangement is required. The drawback of this method is that the oscillator phase noise and the laser amplitude noise can affect the detection result (10).

The frequency of the laser diode can be modulated by its driving current or the temperature around it. This characteristic provides another heterodyne detection possibility. Interferometers using FM laser diodes have been demonstrated for measuring the impurity inside the fiber and the length of the fiber as distributed sensors (11). They are also useful for multiplexed systems.

Other schemes such as that using two or more light beams with different wavelengths, that using an amplitude modulator rather than a phase modulator, and that using passive compensation with quarter-wave plate are also found in some interferometers.

Fabry–Perot Interferometer

The Fabry–Perot interferometer consists of two parallel plates whose inner surfaces are coated with partially transparent high-reflectivity films, as shown in Fig. 7(a). Light

beams entering the Fabry–Perot cavity will reflect many times between the two plates before going out of the cavity. To generate multireflection in the cavity, the plate surface must have high reflectivity, often >0.9. This can be implemented by coating the surface with multilayer dielectric films.

Because of the multireflection in the Fabry–Perot cavity, the Fabry–Perot interferometer gives rise to sharp bright fringes for transmitted beams and sharp dark fringes for reflected beams. The relations between the output light intensities and the reflectivities are specified by Airy's formulae, which are written as follows:

$$I^{(t)}/I^{(i)} = T^2/[(1-R)^2 + 4R\sin^2(\phi/2)]$$
$$I^{(r)}/I^{(i)} = 4R\sin^2(\phi/2)/[(1-R)^2 + 4R\sin^2(\phi/2)]$$

where $I^{(i)}$ denotes the incident optical intensity, $I^{(t)}$ the transmitted optical intensity, $I^{(r)}$ the reflected optical intensity, R and T are the reflectivity and the transmissivity of the plate surface, respectively, and ϕ is the phase difference of multiple light waves. The finesse is a parameter for specifying the sharpness of the fringes. It is defined as the ratio of the separation distance of adjacent fringes and the half-width of the fringe. The greater the finesse, the smaller the half-width and the narrower the fringes.

For the transmitted rays, the difference of multiple light waves is of the form (4)

$$\phi = (4\pi/\lambda)nL\cos\theta + 2\phi_d$$

where L is the separation distance between the two plates, θ is the incident angle, and ϕ_d is the additional phase change on internal reflection. Conventionally, the Fabry–Perot interferometer with fixed L is referred to as the *Fabry–Perot etalon.*

One application of the Fabry–Perot interferometer is the study of the fine structure of spectral lines. The Fabry–Perot interferometer is suitable for this work because it can give very narrow fringes. In this situation, another parameter, called the free spectral range, is used to specify the upper limit of the wavelength difference between the two light waves. When the wavelength difference approaches this upper limit, the displacement between the two fringe patterns will approach the separation distance of two adjacent fringes of any fringe pattern. Introduction of some auxiliary device, for example, a prism, into the instrument can eliminate this problem.

Another application of the Fabry–Perot interferometer is optical filtering. The Fabry–Perot interferometer only transmits the specific wavelengths that fall into the narrow passband corresponding to the sharp bright fringes. Therefore the Fabry–Perot interferometer can serve as bandpass filter. Use of the PZT element can make this optical filter electrically tunable. In this case, applied voltage makes PZT elements stretch or contract so that the length of the Fabry–Perot cavity as well as its passband are varied.

A typical arrangement of the fiber-optic Fabry–Perot interferometric sensor is shown in Fig. 7(b). The measurand changes the optical path length of the cavity and therefore the phase difference of light beams proceeding to the photodetector. The fiber-optic Fabry–Perot interferometric sensors are suitable for measurements of temperature, pressure, and vibration. The materials of the Fabry–Perot cavity can be different from those of the optical fiber, which makes possible the application of the fiber-optic Fabry–Perot interferometric sensor to some specific measurements. Reference (12) gives an example of high temperature measurement. In this case, the sensor is a ceramic Fabry–Perot cavity connected by a multimode uncoated sapphire fiber. The report showed that it attained a resolution of 0.2°C over a range of 310° to 970°C.

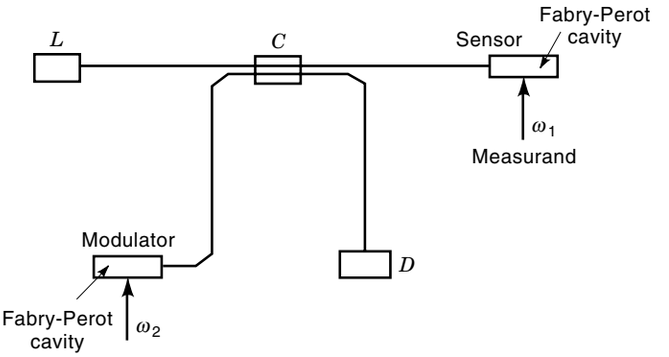

Figure 8. The arrangement of the extrinsic fiber-optic Fabry–Perot interferometer. There are two Fabry–Perot cavities in this system; one is a sensor and one is a modulator. L, laser; C, coupler; D, photodetector.

Since there is no separated reference arm for the fiber-optic Fabry–Perot interferometer, a particular phase bias arrangement should be designed. Figure 8 shows an example of this. There are two Fabry–Perot cavities in this system, one is used as the remote sensor and the other as the modulator. The two Fabry–Perot cavities are modulated at two different frequencies, respectively. The output of the photodetector is the sum of the infinitely many harmonic terms. In this output the phase shift induced by the measurand can be determined by use of the Bessel recurrence relation. This detection system can eliminate the influences due to source intensity variation, fringe contrast fluctuation, and random phase drift and provide a linear readout of the phase shift (13).

FIBER-OPTIC SAGNAC INTERFEROMETER

The Sagnac interferometer is an instrument that detects the nonreciprocal phase difference of two counterpropagating lightwaves. The measurement of rotation rate as a gyro is perhaps the most important application of this interferometer. The basic configuration of the fiber-optic gyro is shown schematically in Fig. 9. The rotation of the fiber coil about its axis makes the two optical paths unequal for the two counterpropagating beams so that a nonzero phase difference is produced between the two light waves. It can be verified that this Sagnac phase difference is

$$\phi = 8\pi NA\Omega/\lambda c$$

where Ω is the rotation rate, and N and A are the number of turns and the area of the fiber coil, respectively (14). This phase difference is nonreciprocal. Its magnitude and sign depend on the rotation rate and direction. Nevertheless, since the interference intensity varies with $\cos\phi$, the sensitivity fades completely as the rotation rate approaches zero. Moreover, the rotation direction cannot be discriminated in terms

of the output of the photodetector in this situation. To solve this problem, several methods have been devised to introduce a nonreciprocal 90° phase bias into the system.

The detection schemes for the fiber-optic gyro are classified as open-loop scheme and closed loop scheme. Figure 9 shows an open-loop system. It is an all-fiber phase-bias gyroscope. An ac phase modulator PZT is inserted into the fiber loop to introduce 90° phase bias. It seems that this modulator cannot produce the nonreciprocal phase bias because the changes in paths would be identical for the two light waves. However, in practice, as the two counterpropagating light waves pass through the PZT device at different moments, the path lengths for the two lightwaves are different. The relation between the output and the phase difference is similar to that shown in Eq. (2). In this case, fiber polarizers and polarization controllers may be required to maintain the identical polarization paths. The main feature of this arrangement is that all its components are constructed on a continuous optical fiber. This helps to remove the noise caused by reflections at the joints of components. The experiment shows that this interferometer has a phase error of 2×10^{-6} rad, corresponding to 0.2°/h of long-term stability (15).

Figure 10 shows a phase-nulling fiber-optic gyroscope. A frequency modulator rather than the phase modulator is used in this closed-loop system. The two light waves counterpropagate along the fiber coil before and after passing through the frequency modulator, and produce a beat-frequency signal that reflects Sagnac phase shift. Through the feedback system, this beat-frequency signal makes the frequency change in such a way that the phase shift due to this frequency change just nulls out the Sagnac phase shift. There are two difficulties involved in this scheme: one is the need for a low frequency modulator and the other is about the dispersion of fiber. Some methods are available for eliminating these problems (3).

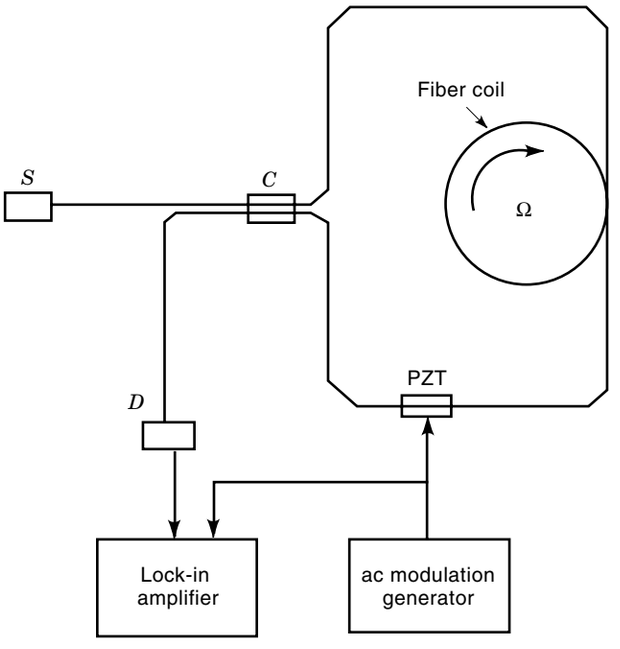

Figure 9. The basic structure of the fiber-optic Sagnac interferometer with phase bias. It is an open-loop system. The phase modulator is placed close to one end of the fiber coil to produce effective phase modulation. *S*, optical source; *C*, coupler; *D*, photodetector.

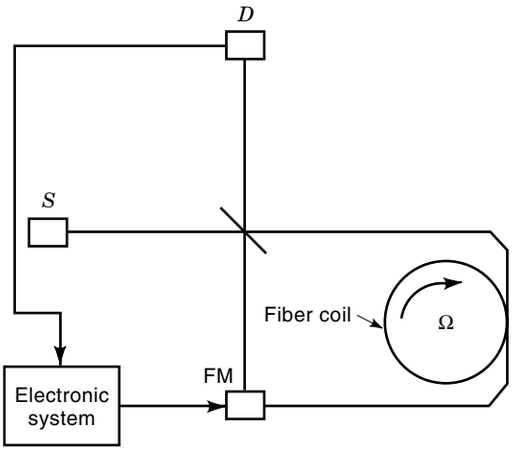

Figure 10. The typical arrangement of the phase-nulling fiber-optical gyro, where the frequency modulator rather than the phase modulator is used. *S*, optical source; *D*, photodetector; FM, frequency modulator.

The heterodyne scheme can also be used to detect the Sagnac phase shift. In this system, a frequency modulator such as the Bragg cell is employed to modulate the frequency. The FM signal with an intermediate frequency includes the information of the Sagnac phase shift. The electronic circuit discriminates this FM signal. To prevent the influence of backscattering light waves, a coding technique by which the modulation frequency varies in a triangular fashion is used. The heterodyne system can eliminate the influence of the $1/f$ noise and avoid the AM effect (16).

A special problem for the Sagnac interferometer is the influence of coherent backscattering light waves that result in unwanted interference. One method to eliminate this influence is the use of incoherent sources such as the superluminescent diode, which emits short-coherence-length light.

Besides rotation rate, other factors such as current can produce nonreciprocal phase difference in the fiber-optic Sagnac interferometer. The current passing across the fiber coil generates a magnetic field. The Faraday effect induces a nonreciprocal phase shift between the two circularly polarized light waves counterpropagating through the fiber coil. It is verified that this nonreciprocal phase shift is proportional to the current. Many practical disturbances to the measurement can influence the measurement accuracy. P-A. Nicati et al. have analyzed disturbances to the Sagnac interferometer (17).

The Twyman–Green interferometer is the variant of the Michelson interferometer. Figure 11 shows the basic form of the Twyman–Green interferometer. It uses broad beams, and it can be used to test the parallelism of the wave fronts of two light waves. The observer will see a uniform illumination if the two wave fronts are parallel and distinct fringes if there is some distortion between them. The fringes will shift as the mirror moves. The shifting direction is related to the distortion direction. The feature of this interferometer makes it possible to test the surface flatness of large objects.

Heterodyne detection scheme and image sensors such as the CCD linear array and area array are usually employed to receive the spatially distributed fringes produced by the

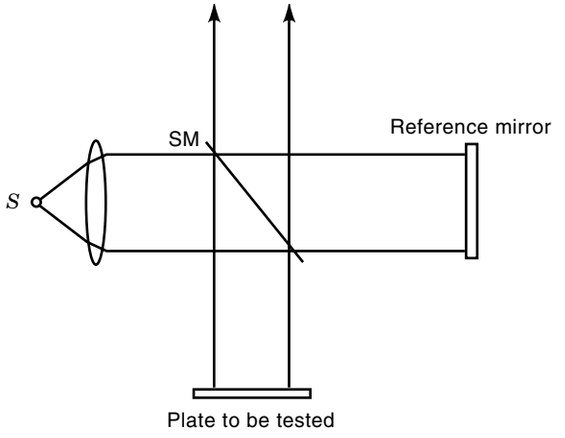

Figure 11. The basic form of the Twyman–Green interferometer, which is used to test the deformation of the plate. *S*, light source; SM, semireflecting, semitransmitting mirror.

Twyman-Green interferometer. The heterodyne detection system transforms the sign of the phase difference, which depends on the distortion direction of the tested surface, to the sign of the time difference of the zero crossing of the sensing signal and that of the reference signal. Thus the spatial distortion of the surface can be determined by measuring the temporal phase difference between the sensing signal and the reference signal (18).

The fiber-optic dual-mode interferometer is a one-fiber interferometer, that is, there are two modes propagating in only one fiber rather than one mode propagating in two separate fibers. This kind of interferometer is useful in temperature and pressure measurements. The variation of the temperature leads to the variation of the phase difference between the two modes and therefore makes a fringes shift. W. Eickhoff has demonstrated a scheme for measuring temperature which used the highly and linearly birefringent fiber with internal lateral stress and had a sensitivity of $1.66\ \text{rad} \cdot \text{K}^{-1} \cdot \text{m}^{-1}$. The advantage of such an interferometer is that variation of source intensity does not influence the readout (19).

In the resonant ring interferometer the output beam reenters the interferometer to produce resonance. Because there is multiple-beam interference in the ring, this interferometer, like the Fabry–Perot, can give rise to sharp fringes. It can measure various parameters with high sensitivities and resolutions. Figure 12 shows two basic forms of the resonant ring interferometer (20).

Other interferometers such as Young's interferometer and the Jamin interferometer are also useful in practical applications (1).

RECENT DEVELOPMENTS

Many effective interferometric schemes have been advanced during the past decade. White-light interferometers utilize wideband light sources. With white light it is possible to discriminate the zeroth-order fringe readily and thereby make absolute measurements. T. Li et al. have given an example of the white-light Michelson interferometer for absolute distance measurement (21). With a heterodyne scheme a two-Mach–Zehnder interferometer combination also can be used for absolute distance measurement (22). The digital technique has been incorporated with the interferometer. The digital integrating interferometer (23) is an electronic feedback-controlled system using digital feedback technique to control phase tracking. A compact interferometer with a PC interface has been reported for displacement measurement (24).

The measurement abilities of the interferometer have been largely expanded. Besides displacement, length, vibration, temperature, pressure, strain, acoustic wave, current, magnetic field, and rotation rate, applications of interferometers to measurements of the gravitation and the fifth force (25,26), bending (27), energized electric cable underground (28), hydrocarbon pollutants in the bulk of the liquid (29), and dipole-orientation distributions of a polymer (30), have been reported.

The interferometric spectrometer has aroused a great deal of interest. S-J. Chern et al. introduced an enhanced Michelson interferometer incorporated in a modified forward-backward linear prediction algorithm. It eliminates the drawbacks of conventional FFT method that involves a large amount of calculation (31). For spectrum measurement, it has been reported that use of the correlated unbalanced interferometric method can attain a resolution 100 times better than that of the Fabry–Perot interferometer, which is able to reach a resolution of the order of 0.5 kHz in some special situations (32). Some research work shows that the Fabry–Perot interferometer is a low-pass device to time varying optical input (33). Longer cavity can provide higher spectral resolution, but may result in worse dynamic response. Similar conclusions can be drawn for the ring interferometer.

Another development related to spectral devices is the electrically tunable optical filter, which is useful in communication systems for wavelength division multiplexing. In 1990, J. S. Patel et al. reported a Fabry–Perot interferometric filter whose cavity is filled with a nematic liquid-crystal material.

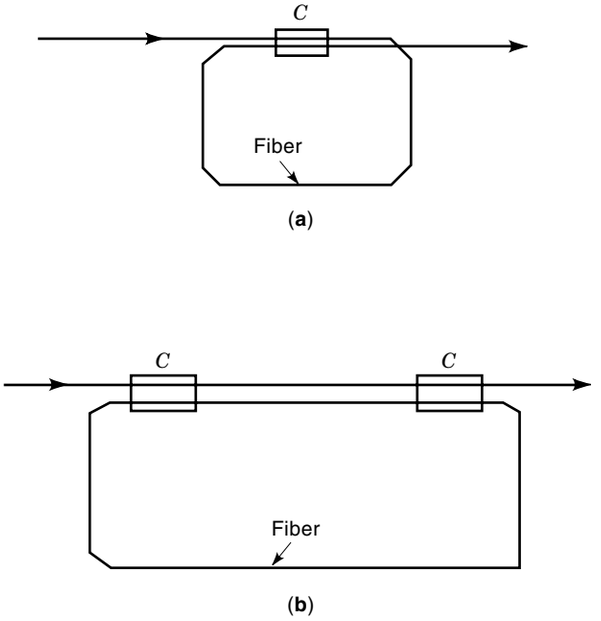

Figure 12. Two forms of resonant ring interferometers, in which a portion of output light is fed back into the interferometer. *C*, couplers.

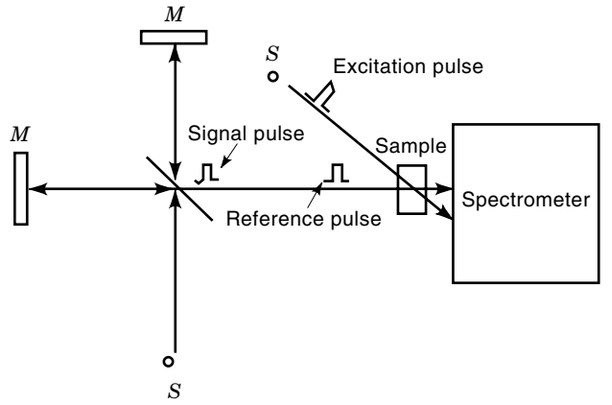

Figure 13. The frequency-domain interferometer for study of femtosecond phase spectroscopy. S, optical source; M, mirror.

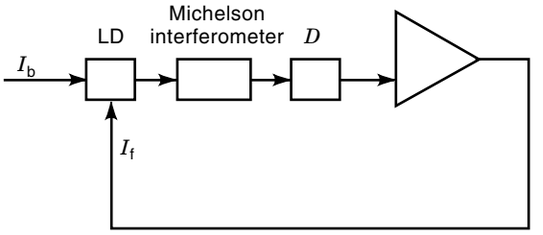

Figure 14. The hybrid bistable and multistable interferometer. LD, laser diode; D, photodetector; I_b, bias current; I_f, feedback current.

The voltage applied to the device regulates the refractive index of the material in the cavity, rather than the length of the cavity, to change the pass band. This kind of electrically tunable optical filter has a simple structure. It consumes less power than conventional devices. However, it is polarization sensitive. An improvement has been made by using the same material but with twisted structure. In this case, when applied voltage was relatively high (≈2 V), the device was polarization insensitive. The experiment showed that the line width of the transmission peak of this device is about 0.5 nm. Its response time is of the order of millisecond. Further research results have shown that the substitution of the ferroelectric liquid-crystal for the nematic liquid-crystal can increase the response speed of this kind of optical filter (34).

Similar to the interference in the time domain, interference can occur in the frequency domain between two light waves. One can see this phenomenon even if two light wave trains are separated by a time interval longer than the wave train duration. Figure 13 schematically shows a frequency-domain interferometer useful for the study of femtosecond phase spectroscopy. There are three pulses propagating in this interferometer: probe, excitation, and reference. They pass through the same sample at different moments. The reference pulse passes through the sample first, then the excitation pulse, and finally the probe pulse. The reference pulse does not undergo change in the complex refractive index caused by the excitation pulse but the probe pulse does. One can determine the femtosecond phase spectrum in terms of the interference between the probe and the reference pulses with and without excitation. The advantage of this method is that there is no need to temporally overlap the femtosecond pulses accurately (35).

K. Misawa and T. Kobayashi advanced another femtosecond interferometer. They designed a Sagnac interferometer for measurement of continuous phase spectra with white light. The zeroth-order fringe of white light can be found readily in the Sagnac interferometer because of its reciprocal structure. The sample is inserted into the optical loop. The reference pulse arrives at the sample earlier than both the excitation and the probe pulses. The probe and the reference pulses propagate in opposite directions, and the probe pulse reaches the sample after the excitation pulse passes through it. According to the interference results between the probe pulse and the reference pulse, one can estimate the nature of the sample (36).

Besides the measurement of the femtosecond phase spectra the femtosecond interferometer can be employed to study the collision between two solitons (37).

The nonlinear or digital performance of the interferometer is an attractive research area. Figure 14 shows the block diagram of a hybrid bistable and multistable interferometer (38). With the help of electronic feedback, the interferometer can be operated in bistable or multistable state. In this case, the external light input minus the output of the interferometer controls the injection current of the laser diode. The bistable and multistable states are observed in the output from the laser diode. Besides this hybrid arrangement, all-optical devices such as the twin-core fiber nonlinear Mach–Zehnder interferometer (39) and the bistable fiber-optic unbalanced Michelson interferometer (40) are available for bistable operation. M. Jinno and T. Matsumoto reported a nonlinear Sagnac interferometer. The highly stable logic operations including INVERSION, AND, OR, XOR were observed at the rate of multigigabit operations per second (41).

Some new bistable schemes have been discussed recently. Figure 15 shows a fiber-reflection Mach–Zehnder interferometer. It is able to switch the light from reflection to transmission or vice versa by changing the phase difference of lightwaves when couplers have splitting ratios in a range ($0.146 < \kappa < 0.854$). Beyond this range the interferometer transmits most of the light and reflects a small portion of light, a feature that will make this interferometer useful for optical switching (42).

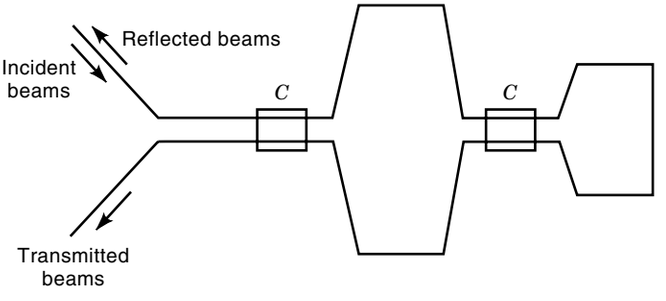

Figure 15. The configuration of the fiber-reflection Mach–Zehnder interferometer. C, couplers.

BIBLIOGRAPHY

1. B. Culshaw, *Optical Fiber Sensing and Signal Processing,* London: Peter Peregrinus Ltd., 1984.
2. T. G. Giallorenzi et al., Optical fiber sensor technology, *IEEE J. Quantum Electron.,* **QE-18**: 626–665, 1982.
3. S. L. Chuang, *Physics of Optoelectronic Devices,* New York: Wiley, 1995.
4. M. Bass, *Handbook of Optics,* New York: McGraw-Hill, 1995.
5. T. Kimura et al., Heat propagation in differential thermal analysis using fiber-optics technology, *IEEE Trans. Instrum. Meas.,* **IM-38**: 599–603, 1989.
6. D. A. Jackson, A. Dandridge, and S. K. Sheem, Measurement of small phase shifts using a single-mode optical-fiber interferometer, *Opt. Lett.,* **5**: 139–141, 1980.
7. K. P. Koo, A. B. Tveten, and A. Dandridge, Passive stabilization scheme for fiber interferometers using (3×3) fiber directional couplers, *Appl. Phys. Lett.,* **41**: 616–618, 1982.
8. A. Dandridge, A. B. Tveten, and T. G. Giallorenzi, Homodyne demodulation scheme for fiber optic sensors using phase generated carrier, *IEEE Trans. Microw. Theory Tech.,* **MTT-30**: 1635–1641, 1982.
9. V. S. Sudarshanam and K. Srinivasan, Linear readout of dynamic phase change in a fiber-optic homodyne interferometer, *Opt. Lett.,* **14**: 140–142, 1989.
10. J. H. Cole, B. A. Danver, and J. A. Bucaro, Synthetic-heterodyne interferometric demodulation, *IEEE J. Quantum Electron.,* **QE-18**: 694–696, 1982.
11. R. Juskaitis et al., Distributed interferometric fiber sensor system, *Opt. Lett.,* **17**: 1023–1025, 1992.
12. A. Wang et al., Sapphire-fiber-based intrinsic Fabry–Perot interferometer, *Opt. Lett.,* **17**: 1021–1023, 1992.
13. V. S. Sudarshanam and R. O. Claus, Split-cavity cross-coupled extrinsic fiber-optic interferometric sensor, *Opt. Lett.,* **18**: 543–545, 1993.
14. W. K. Burns, *Optical Fiber Rotation Sensing,* San Diego: Academic, 1994.
15. R. A. Bergh, H. C. Lefevre, and H. J. Shaw, All-single-mode fiber-optic gyroscope, *Opt. Lett.,* **6**: 198–200, 1981.
16. B. Culshaw and I. P. Giles, Frequency modulated heterodyne optical fiber Sagnac interferometer, *IEEE J. Quantum Electron.,* **QE-18**: 690–693, 1982.
17. P-A. Nicati and P-A. Robert, Numerical analysis of second-order polarization effects in a Sagnac current sensor, *IEEE Trans. Instrum. Meas.,* **IM-39**: 219–224, 1990.
18. N. A. Massie, R. D. Nelson, and S. Holly, High performance real-time heterodyne interferometry, *Appl. Opt.,* **18**: 1797–1803, 1979.
19. W. Eickhoff, Temperature sensing by mode-mode interference in birefringent optical fibers, *Opt. Lett.,* **6**: 204–206, 1981.
20. K. Arai et al., Sensitivity-enhancing scheme of a polarimetric heterodyne sensor using a birefringent fiber loop, *Opt. Lett.,* **15**: 1103–1105, 1990.
21. T. Li, A. Wang, K. Murphy, and R. O. Claus, White-light scanning fiber Michelson interferometer for absolute position-distance measurement, *Opt. Lett.,* **20**: 785–787, 1995.
22. E. Gelmini, U. Minoni, and F. Docchio, Tunable, double-wavelength heterodyne detection interferometer for absolute-distance measurements, *Opt. Lett.,* **19**: 213–215, 1994.
23. K. Toyama et al., Digital integrating fiber-optic gyroscope with electronic phase tracking, *Opt. Lett.,* **16**: 1207–1209, 1991.
24. S. Donati, L. Falzoni, and S. Merlo, A PC-interfaced compact laser-diode feedback interferometer for displacement measurements, *IEEE Trans. Instrum. Meas.,* **IM-45**: 942–947, 1996.
25. K. Kuroda and N. Mio, A free fall interferometer to search for a possible fifth force, *IEEE Trans. Instrum. Meas.,* **IM-38**: 196–199, 1989.
26. J-M. Chartier et al., A portable iodine stabilized He-Ne laser and its use in an absolute gravimeter, *IEEE Trans. Instrum. Meas.,* **IM-42**: 420–422, 1993.
27. C. E. Covington, J. Blake, and S. L. A. Carrara, Two-mode fiber-optic bending sensor with temperature and strain compensation, *Opt. Lett.,* **19**: 676–678, 1994.
28. A. V. Mamishev et al., Nonintrusive sensing techniques for the distribution of energized electric cables, *IEEE Trans. Instrum. Meas.,* **IM-45**: 457–461, 1996.
29. D. P. Hand et al., Optical fiber interferometry for photoacoustic spectroscopy in liquids, *Opt. Lett.,* **20**: 213–215, 1995.
30. W. Brinker et al., Phase-shift interference microscope for the investigation of dipole-orientation distributions, *Opt. Lett.,* **20**: 816–818, 1995.
31. S-J. Chern and K-J. Chao, An enhanced Fourier transform spectrometer with a search algorithm, *IEEE Trans. Instrum. Meas.,* **IM-45**: 127–135, 1996.
32. I-W. Oh and H. R. D. Sunak, Measurement of the spectral linewidth of semiconductor laser for use with coherent optical communication system, *IEEE Trans. Instrum. Meas.,* **IM-36**: 1054–1059, 1987.
33. P. Tremblay and R. Ouellet, Frequency response of a Fabry–Perot interferometer used as a frequency discriminator, *IEEE Trans. Instrum. Meas.,* **IM-40**: 204–207, 1991.
34. J. S. Patel, Electrically tunable ferroelectric liquid-crystal Fabry-Perot filter, *Opt. Lett.,* **17**: 456–458, 1992.
35. E. Tokunaga and A. Terasaki, Frequency-domain interferometer for femtosecond time-resolved phase spectroscopy, *Opt. Lett.,* **17**: 1131–1133, 1992.
36. K. Misawa and T. Kobayashi, Femtosecond Sagnac interferometer for phase spectroscopy, *Opt. Lett.,* **20**: 1550–1552, 1995.
37. Y. Sakai, R. J. Hawkins, and S. R. Friberg, Soliton-collision interferometer for the quantum nondemolition measurement of photon number: Numerical results, *Opt. Lett.,* **15**: 239–241, 1990.
38. J. Ohtsube and Yun Liu, Optical bistability and multistability in an active interferometer, *Opt. Lett.,* **15**: 731–733, 1990.
39. B. K. Nayar et al., All-optical switching in a 200 m twin-core fiber nonlinear Mach-Zehnder interferometer, *Opt. Lett.,* **16**: 408–410, 1991.
40. N. Furstenau, Bistable fiber-optic Michelson interferometer that uses wavelength control, *Opt. Lett.,* **16**: 1896–1898, 1991.
41. M. Jinno and T. Matsumoto, Ultrafast all-optical logic operations in a nonlinear Sagnac interferometer with two control beams, *Opt. Lett.,* **16**: 220–222, 1991.
42. G. Dickinson, D. A. Chapman, and D. A. Gorham, Properties of the fiber reflection Mach-Zehnder interferometer with identical couplers, *Opt. Lett.,* **17**: 1192–1194, 1992.

KEN XU
Huazhong University of Science and Technology

INTERFEROMETERS, ACOUSTIC. See ACOUSTIC WAVE INTERFEROMETERS.

INTERFEROMETRY. See INTERFEROMETERS.

INTERFEROMETRY, SPECKLE. See ELECTRONIC SPECKLE PATTERN INTERFEROMETRY.

INTERIOR POINT METHODS. See CONVEX OPTIMIZATION.